ARTICLE

Tailoring Silica Nanotribology for CMP Slurry Optimization: Ca^{2+} Cation Competition in $C_{12}TAB$ Mediated Lubrication

Ivan U. Vakarelski,[*,†,‡] Scott C. Brown,[*,†] G. Bahar Basim,[†,§] Yakov I. Rabinovich,[†] and Brij M. Moudgil[†]

Particle Engineering Research Center and Department of Materials Science & Engineering, University of Florida, P.O. Box 116135, Gainesville, Florida 32611, Institute of Chemical and Engineering Sciences, 1 Pesek Road, Jurong Island, 627833, Singapore, and Department of Mechanical Engineering, Ozyegin University, Altunizade, Istanbul

ABSTRACT Self-assembled surfactant structures at the solid/liquid interface have been shown to act as nanoparticulate dispersants and are capable of providing a highly effective, self-healing boundary lubrication layer in aqueous environments. However, in some cases in particular, chemical mechanical planarization (CMP) applications the lubrication imparted by self-assembled surfactant dispersants can be too strong, resulting in undesirably low levels of wear or friction disabling material removal. In the present investigation, the influence of calcium cation (Ca^{2+}) addition on dodecyl trimethylammonium bromide ($C_{12}TAB$) mediated lubrication of silica surfaces is examined via normal and lateral atomic force microscopy (AFM/LFM), benchtop polishing experiments and surface adsorption characterization methods. It is demonstrated that the introduction of competitively adsorbing cations that modulate the surfactant headgroup surface affinity can be used to tune friction and wear without compromising dispersion stability. These self-healing, reversible, and tunable tribological systems are expected to lead to the development of smart surfactant-based aqueous lubrication schemes, which include designer polishing slurries and devices that take advantage of pressure-gated friction response phenomena.

KEYWORDS: chemical mechanical planarization (CMP) • atomic force microscopy (AFM) • tribology • surfactants

INTRODUCTION

Surfactant aggregates are commonly used as dispersants, grinding aids, collectors, emulsifiers, wetting agents, etc., in particulate processing schemes (1−6). An important function of self-assembled surfactant structures forming on a solid/liquid interface has been to promote stability in colloidal systems. Adsorbed surfactant structures have been shown to provide robust stability in extreme chemical and/or physical environments by invoking self-healing steric and electro-steric repulsive force (4−10). Self-assembled surfactant structures are also known to be effective boundary lubricants (11−16); however, the lubrication that results from the incorporation of self-assembled surfactant structures for dispersion is not always beneficial (11). Friction, though sometimes resulting in adverse affects, is often a necessary component of numerous industrial processes such as dewatering and polishing, and is an important design parameter for the development of current and future consumer and manufacturing products and devices including microscale and nanoscale electromechanical systems (MEMS and NEMS), biomedical implants, and designer chemical mechanical polishing/planarization (CMP) slurries (17−23).

Previously, we demonstrated that physisorbed alkyl quaternary amine surfactants are capable of providing extensive lubrication of silica surfaces at loading forces that well exceed the critical pressure required to rupture micellar structures residing at the solid/liquid interface (13). The lubrication induced from these surfactants is believed to be mediated by a residual molecular surfactant film. The presence of this film subsequent to pressure-induced micelle degradation has been supported by molecular dynamic simulations as well as nanotribology experiments (13, 24, 25).

Flexibility in designing both lateral and normal surface interactions could be advantageous in a number of emerging and existing processes. For instance, the CMP process that is used to planarize (i.e., flatten) wafer surfaces for the layer-by-layer assembly and fabrication of devices in the microelectronic industry requires the enhancement of normal repulsive force to promote robust nanoparticulate slurry stability as well as a controlled friction. Herein, we describe the influence of divalent cation species in postcritical micelle concentration (CMC) $C_{12}TAB$ environments. The current research provides an example of how the lateral and normal interaction forces between physisorbed surfactant systems can be precisely modulated to provide tailored tribology through the application of ionic species that effectively compete with surfactants for surface adsorption sites. CMP polishing experiments were used for testing the tribology of

* Corresponding author. Tel: +65 6796 3880 (I.U.V.); (352) 273-1243 (S.C.B.). Fax: +65 6316 6183 (I.U.V.); (352) 846-1196 (S.C.B.). E-mail: ivakarelski@gmail.com (I.U.V.); sbrown@perc.ufl.edu (S.C.B.).
Received for review January 25, 2010 and accepted April 6, 2010
† University of Florida.
‡ Institute of Chemical and Engineering Sciences.
§ Ozyegin University.
DOI: 10.1021/am100070e
© 2010 American Chemical Society

Published on Web 04/12/2010

C_{12}TAB-silica systems, in part because of their sensitivity to modulations in both normal (i.e., particle stability, which impacts surface roughness and defectivity) and lateral forces (i.e., material removal rate). The results that follow demonstrate an example of a self-healing, reversible, and tunable tribological system in an aqueous environment.

EXPERIMENTAL SECTION

Materials. Dodecyl trimethylammonium bromide (C_{12}TAB) surfactant was obtained from Aldrich Chemical Co. and was at least 99% pure. NaCl, CsCl, and $CaCl_2$ employed were of analytical grade and roasted for 4 h at 400 °C to remove organic contaminants. Silica slurries were prepared using Geltech Inc. monosize solgel silica powders. A p-type silicon wafer with a 2 μm thick coating of CVD silica was supplied by Silicon Quest International. The root-mean-square (rms) roughness of the nominal silica surface, as measured by AFM, was between 0.3 and 0.4 nm. Monodispersed nonporous silica spheres (7.5 μm) were purchased from Bangs Laboratories Ltd. The water for all experiments was produced by a Millipore filtration system and had an internal specific resistance less than 18.2 MΩ.

Slurry Preparation and Polishing Tests. The polishing slurries were prepared using 0.2 μm monosize solgel silica powder (Geltech Inc.) and DI water. All slurries were maintained at pH 10.5 through the addition of NaOH and had a final silica solids loading of 12 wt %. The baseline slurry consisted of 12 wt % silica in pH 10.5 DI water and was used to compare the relative polishing performance of the slurries developed in this study. Test slurries were mechanically dispersed through sonication in pH 10.5 DI water. To prepare stable slurries at high ionic strength, we first added the desired amount of C_{12}TAB surfactant to a suspension of silica particles in pH 10.5 DI and subsequently sonicated. Afterward, the intended additional amount of electrolyte was added to the slurry followed by a final pH adjustment to 10.5. To monitor the dispersion and stability of the slurries, we performed particle size analysis measurements via light scattering using a Coulter LS 230 instrument. The background water used to run the size analysis experiments was prepared to have the same chemical composition as the modified slurries.

Eight inches wafers were obtained from Silicon Quest International and were cut into square samples of 1.0 × 1.0 in. A Struers Rotopol 31 tabletop polisher was used for polishing with IC 1000/Suba IV stacked pads supplied by Rodel Inc. A schematic of the polishing test experimental setup is given in Figure 1. A grid-abrade diamond pad conditioner was used to abrade the pad before each polishing test. The down force was adjusted to 7.0 psi (492 g/cm^2) and the rotation speed was 150 rpm for both the pad and the wafer. The thickness of the oxide film on the wafers was measured using a spectroscopic ellipsometry method, before and after the polishing, to calculate the removal rate. The slurry flow rate was 100 mL/min and the polishing tests were conducted with 50 mL slurries for 30 s at a solid concentration of 12 wt %. Atomic force microscopy (AFM) was used for surface roughness and deformation analysis of the polished wafers. A minimum of four polishing tests were conducted for all conditions and five 5 × 5 μm^2 size images were taken for each polished wafer to evaluate the root-mean-square (rms) surface roughness and maximum surface deformation (maximum depth of scratches or pits on the surface, R_{max}) responses.

Frictional and Normal Force Measurements. All interaction force measurements including frictional/lateral force measurements were performed using a Digital Instruments Nanoscope III MultiMode atomic force microscope equipped with a fused silica liquid cell. Rectangular tipless cantilevers (MikroMasch) with a normal spring constant in the range of $K_N = 2.8 \pm 0.3$ N/m were used for all interaction force experiments. The exact values of the normal spring constants were determined by the frequency method (26). Silica particles were attached to the cantilever end using a small amount of high-temperature melting epoxy (Shell Epikote 1009). Forces normal to the flat surface were measured by the standard colloidal probe method procedure (27).

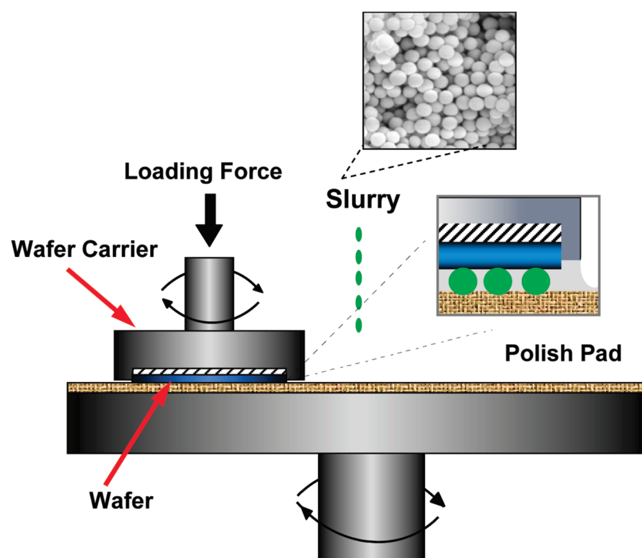

FIGURE 1. Schematic representation of the CMP polishing system. The inset shows a SEM image of 0.2 μm silica slurry particle that were used as the abrasive in the current research.

The frictional, also referred to as lateral force microscopy (LFM), measurements were performed using the "friction force" mode of the MultiMode AFM. In this mode, the colloidal probe is pressed against the substrate at a constant applied load while the substrate slides horizontally underneath the cantilever. Further details of the measurement procedure are given elsewhere (13, 27−29). The magnitude of the frictional force, F_L, was determined from half of the difference in the lateral force detector signal in one complete scan (cycle), V_L, according to eq 1

$$F_L = \frac{1}{2} V_L S_L \frac{K_L}{H} \tag{1}$$

where S_L is the lateral detector sensitivity, K_L is the lateral spring constant, and H is the distance from the bottom of the sphere to the midpoint of the cantilever. The lateral sensitivity of the detector was determined to be $S_L = 3.1 \times 10^{-4}$ rad/V (30) and the lateral spring constant $K_L = 11.0 \pm 1.3$ nNm/rad was calculated from the experimental value of the normal spring K_N, and the cantilever dimensions (13).

Before each experiment, the silica wafer samples were rigorously washed with acetone, ethanol and water. Colloidal probes were washed with ethanol and water. Both the colloidal probe and the wafer sample were then exposed for 1 h to a short wave UV source.

Surfactant Adsorption Experiments. Surfactant adsorption measurements were performed by two different methods. C_{12}TAB absorption on silica slurry particles in the presence and absence of electrolyte was determined by the solution depletion method using the Wilhelmy plate surface tension method to quantify the concentration of free surfactant in the bulk solution. Briefly, a known concentration of surfactant and electrolyte was mixed with a 12 wt % particle suspension, equilibrated, and centrifuged to separate the supernatant from the surfactant-coated particles. The residual surfactant concentration in the

supernatant was then determined by surface tension measurements. The absorbed surfactant concentration is determined from the difference of starting and supernatant concentration values. Surfactant concentration versus surface tension calibration curves were obtained for a range of electrolyte concentrations.

Relative surfactant adsorption measurements were also performed using Fourier transform infrared spectroscopy in attenuated internal reflection (FT-IR/ATR) mode. FT-IR experiments were conducted with a nitrogen-purged Nicolet Magna 760 spectrometer equipped with a DTGS detector. A silicon ATR crystal with silica layer on the surface was used for this analysis, on which 256 coadded scans were collected at a resolution of 4 cm^{-1} for all the solution conditions. The intensity of the CH_2 peaks of the $C_{12}TAB$ surfactant (at 32 mM concentration) was recorded at 3000−2750 cm^{-1} wavelength ranges. The background spectrum was the single-beam spectrum of the dry silicon crystal with a silica surface layer. The relative adsorption intensity was analyzed by comparing the peak heights of the obtained spectra (6).

Reversibility of Ca^{2+} Cation Adsorption. The reversibility of calcium cation adsorption (and absence of chemisorption) was determined by X-ray photoelectron spectroscopy (XPS) and interpreted by LFM measurements. Briefly, silica wafer samples were immersed and equilibrated in 32 mM $C_{12}TAB$ solutions with 0.2 M $CaCl_2$ at pH 10.5. Some samples of the wafers were removed and blown dry with purified nitrogen gas. Others were first rinsed with DI water then blown dry. The presence of calcium on the silica wafer surface was determined by XPS using a Perkin-Elmer 5100 XPS system equipped with Mg Ka radiation (1253.6 eV). Results were compared between preparations and a control wafer sample.

Lateral force measurements were performed as described above between a silica particle and silica wafer in deionized water adjusted to pH 10.5 over a range of loading forces. Subsequently the liquid cell was flushed with 32 mM $C_{12}TAB$ and 0.2 mM $CaCl_2$ at pH 10.5 and the frictional force for an identical loading regime was measured. The liquid cell was then returned to the original pH 10.5 adjusted DI water system by flushing and the frictional force versus loading force curve was once again measured and compared to the previously collected data.

RESULTS AND DISCUSSION

CMP Polishing Experiments. Silica CMP is typically performed in alkaline environments (~pH 10.5) applying nanoscale to submicrometer silica particle dispersions as the abrasives. Solgel silica slurries tend to aggregate in the high ionic strength environment commonly found in CMP leading to excessive surface roughness in addition to unacceptable levels of surface defects. In previous investigations, it was illustrated that the addition of postmicellar concentrations of $C_{12}TAB$ leads to slurry stability even in saturated simple electrolyte systems. However, this dispersion was also accompanied by negligible surface polishing, which is inadequate for CMP applications (11).

To design systems for tailored polishing/tribological performance, we used colloidal probe AFM/LFM to identify the origins of the lubrication process imparted by alkyl quaternary amines on silica in aqueous solution. In these experiments, it was determined that the surfactant-surface anchoring strength is the principle determinant for the critical pressure at which the system switches from low friction coefficient residual surfactant layer mediated friction (boundary layer lubrication) to higher friction coefficient regime (bare surface contact) when the silica surface can contact directly (13). In particular, addition of NaCl electrolyte or lowering of the solution pH were shown to decrease the pressure at which the system transitioned to high friction mode. Herein trying to reduce the barrier for the frictional engagement between the silica surfaces in the presence of surfactant, several cations of different states of hydration and valences were screened. From these initial tests, it was found that bivalent cations could significantly improve the polishing performance of silica. Calcium chloride ($CaCl_2$) based surfactant slurries, in particular, were extensively investigated demonstrating the applicability of adsorption site-competition for enhanced and controlled polishing performance.

Table 1. Summary of the Polishing Performance of the Baseline (with and without $CaCl_2$), and $C_{12}TAB$ Mediated Slurries in the Presence of 0.6 M NaCl and 0.1 and 0.2 M $CaCl_2$

	mean particle size (μm)	material removal rate (Å/min)	surface roughness rms (nm)	maximum defect depth R_{max} (nm)
Baseline				
W/O electrolyte	0.2 ± 0.003	3800 ± 250	0.8 ± 0 0.3	25
0.2 M $CaCl_2$	3.5 ± 0.6	6800 ± 302	3.1 ± 1.2	60
32 mM $C_{12}TAB$				
0.6 M NaCl	0.2 ± 0.004	65 ± 27	0.5 ± 0 0.3	22
0.6 M CsCl	0.2 ± 0.004	75 ± 30	0.6 ± 0 0.3	22
0.1 M $CaCl_2$	0.2 ± 0.004	4100 ± 400	0.4 ± 0 0.4	20
0.2 M $CaCl_2$	0.2 ± 0.006	4800 ± 714	0.5 ± 0 0.7	16

Table 1 summarizes some of the screening benchtop polishing tests results. The stability of the slurries is reflected by the slurry mean particle size. The polishing performance is measured by the material removal rate and surface quality in terms of rms roughness and maximum defect depth obtained by AFM imaging of the polished wafer samples. The baseline slurry without additional electrolyte was well-dispersed, whereas the addition of 0.2 M $CaCl_2$ or 0.6 M NaCl led to rapid coagulation and corresponding unacceptable increase in the polished surface roughness and defect size. In good accordance with our previous investigation slurries containing 32 mM $C_{12}TAB$ (2 × CMC) were stable after the addition of 0.6 M NaCl but showed negligible removal rates (10). Results from slurry rheology (31−33), adhesion measurement (34, 35), and nanotribology (36) indicate that the larger, less-hydrated Cs^+ cations could be more efficient to enhance the engagement between the silica surfaces then the smaller and more strongly hydrated Na^+ cations. Nevertheless, the polishing test with 0.6 M CsCl containing slurries indicated similar material removal rate to that of NaCl containing slurries (Table 1).

In contrast with the monovalent salts the addition of $CaCl_2$ to the $C_{12}TAB$ stabilized slurries proved to be highly effective in increasing the material removal rate and at the same time not compromising the slurries stability or polishing quality. The introduction of 0.1 or 0.2 M $CaCl_2$ to $C_{12}TAB$ stabilized slurries at pH 10.5 resulted in material removal

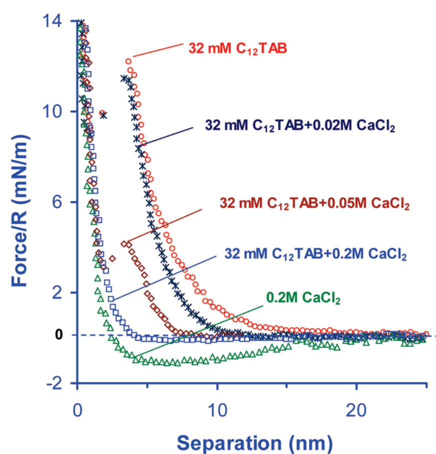

FIGURE 2. AFM normal force measurement between a 7.5 μm silica particle and a silica wafer. Force profiles for the approaching interactions in solutions of pH 10.5 aqueous solutions of 32 mM C_{12}TAB without or with 0.02 M; 0.05 and 0.2 M $CaCl_2$ or 0.2 M $CaCl_2$ without C_{12}TAB.

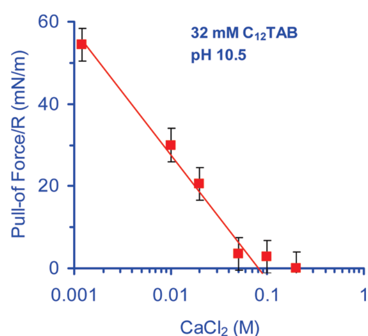

FIGURE 3. Pull-off force between a 7.5 μm silica particle and a silica wafer in pH 10.5 aqueous solutions of 32 mM C_{12}TAB as a function of the added $CaCl_2$ concentration. The left-most point corresponds to the solution without $CaCl_2$. The red line is provided for guidance.

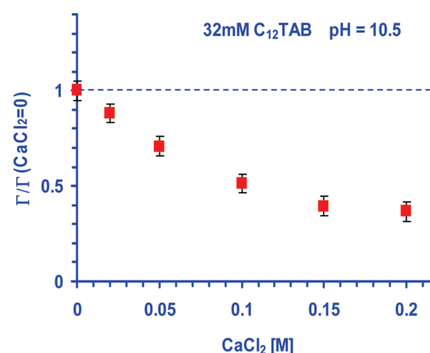

FIGURE 4. Relevant adsorption of C_{12}TAB on silica slurries particle surface in 10.5 pH aqueous solutions of 32 mM C_{12}TAB as a function of the $CaCl_2$ concentration. The dashed line corresponds to the adsorption of 32 mM C_{12}TAB without $CaCl_2$.

rates that exceeded the baseline slurry removal rate values (4100 and 4800 versus 3800 Å/min, respectively) while maintaining acceptable surface deformation parameters.

The polishing test results demonstrate how the general knowledge developed from previous detailed investigations of the surfactant mediated nanotribology and its association with silica CMP performance can be used to develop effective CMP slurry formulations. In the present research, we further investigate the molecular mechanisms behind the enhanced performance of C_{12}TAB/$CaCl_2$ slurries. AFM measurement of the normal interaction force could be related with the slurries stability, whereas lateral interaction force measurements are indicative of the polishing efficiency. Complementary surface characterizations are done by adsorption, FT-IR, and XPS measurement experiments.

Normal Forces and Competitive Adsorption at High pH. To investigate the primary interaction forces related to the slurries stability, we performed a series of AFM colloidal probe force measurement. Figure 2 represents the force curves for the interaction between a silica particle probe and a flat silica surface in solution conditions identical to that of the polishing tests. Figure 3 shows the magnitude of the respective pull-off forces measured during the surface separation. The interaction force curve for 32 mM C_{12}TAB is in good agreement with published force curves for interaction between surfactant aggregate coated surfaces (4−9). An electrosteric repulsive force induced from the interaction between adsorbed surfactant aggregate layers is followed by an abrupt jump-in-contact of the probe to the surface. The later is correlated to the mechanical destruction of the self-assembled surfactant aggregates (9). With the addition of $CaCl_2$ in concentrations up to 0.05 M, the magnitude of the force required to break surface micelles, e.g., the critical repulsive force barrier, is systematically reduced. When the $CaCl_2$ concentration is increased to 0.2 M, the micellar layer breakdown is no longer observed. Nevertheless, during the surfaces' engagement, the interaction is entirely repulsive in accordance with the observed slurry stability. For comparison, the force curve for 0.2 M $CaCl_2$ solution without surfactant passes through a characteristic attractive minimum (van der Waals force secondary minimum) that could be related to the fast coagulation of the slurries without added surfactant.

Previously, we have demonstrated that an increase in monovalent electrolyte (i.e., NaCl) concentration to the C_{12}TAB silica system results in enhanced surfactant cohesion inside the surface-bound micellar assemblies resulting in higher critical repulsive force barriers with increasing electrolyte content (4). This is contrary to the present case for $CaCl_2$, even though the ionic strengths and cation concentrations are similar. We believe that this discrepancy is attributed to the higher affinity of the bivalent Ca^{2+} cations to the silica surface, as compared to the monovalent Na^+ cations, enabling them to effectively compete with C_{12}TAB for surface binding sites. Both Ca^{2+} and C_{12}TAB being cationic ions compete to adsorb electrostatically to the negatively charged deprotonated silanol groups at the silica surface. We can further speculate that because of the competitive adsorption the density of the micellar structures or the number of structure per unit area is decreasing with increasing $CaCl_2$ concentration, which mediates an apparently weaker force barrier response. This theory is supported by the comparative adsorption isotherm presented in Figure 4. Using the solution depletion method detailed in the experimental section we found that the amount of C_{12}TAB adsorbed on the silica slurry particles after the addition 0.2 M $CaCl_2$ leveled to about 40% of the salt free slurries

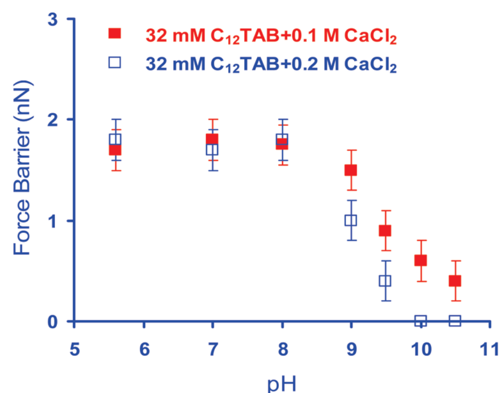

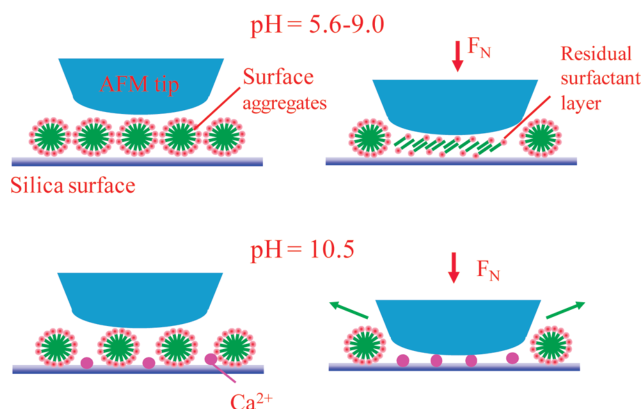

FIGURE 5. Critical force barrier between silica wafer and the AFM tip in aqueous solutions of 32 mM C_{12}TAB and 0.1 and 0.2 M $CaCl_2$ as a function of the solution pH. The cartoons below the graph illustrate the plausible scenarios of the tip engagement with the surface discussed in the text.

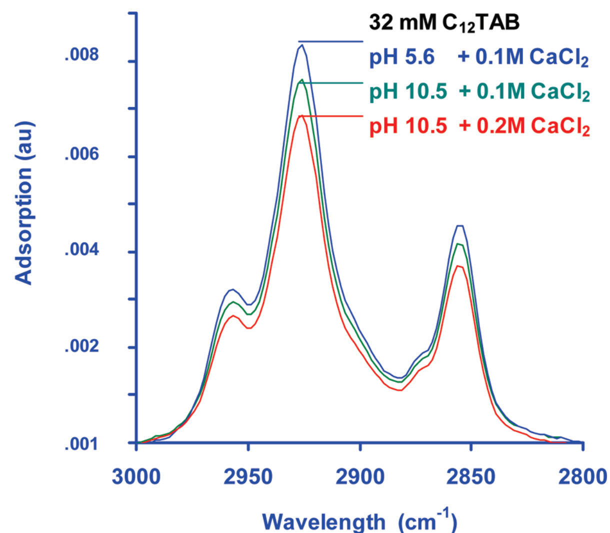

FIGURE 6. FTIR-ATR spectra for C_{12}TAB at 32 mM bulk concentration in the CH_2 stretching region [asymmetric (2920 cm^{-1}), symmetric (2850 cm^{-1})]. The height ratios of the spectra picks correspond to the relevant amount of C_{12}TAB adsorbed on the surface layer. Spectra shown are taken with parallel (p) infrared beam. Ration between the p and s spectra (not shown) is used to determine the order parameter of the adsorbed layer structures (see Singh et al. (6) for details).

adsorption. The sparsely adsorbed structures could lead to increased lateral mobility of the surface structures and eventually to the lack of the jump-in feature in the force curve for 0.2 M $CaCl_2$ when the structure could be completely pushed-out of the contact zone while the surfaces approach and engage (see Figure 5 cartoons). The pull-off force measurements shown in Figure 4 additionally support this hypothesis as indicated by the reduction of the pull-off force with increased $CaCl_2$ content that is a result of the decreasing number and strength of surfactant headgroup attachments to the silica surfaces during separation.

pH Dependence of the Ca^{2+} and C_{12}TAB Competitive Adsorption. Both C_{12}TAB and Ca^{2+} cation adsorption onto silica surfaces are known to increase at higher pH. Whereas C_{12}TAB adsorption modestly increases on silica between pH 8−10.5, Ca^{2+} adsorption is known to dramatically increase around pH 9.0 and above (37, 38). It is then expected that the C_{12}TAB and Ca^{2+} competitive adsorption will be strongly dependent on the solution pH. Here we use AFM critical force barrier measurement in combination with FTIR spectra measurement to investigate C_{12}TAB adsorption dependence with pH in the presence of Ca^{2+} cations.

Figure 5 represents AFM measurement for the critical force barrier between silica surfaces in solutions of 32 mM C_{12}TAB at 0.1 and 0.2 M $CaCl_2$ in the pH range of 5.6 to 10.5. For simplicity, these measurements were taken using a native silicon oxide covered AFM tip instead of the silica particle colloidal probe which should follow the same trend. The data indicate that the repulsive force barrier imposed by the surfactant aggregates significantly reduces at pH 9 and above corresponding with Ca^{2+} cation adsorption. In accordance with the previous section, normal force measurements indicate a lowering of the force barrier when approaching to pH 10.5 at high $CaCl_2$ concentration in accordance with corresponding adsorption data. This can be interpreted to be due to a reduced number of micellar aggregates on the surface with increased pH enabling lateral movement of the aggregates during force interrogation. This is schematically shown by the cartoon insert below Figure 5.

The same trend for competitive C_{12}TAB vs Ca^{2+} adsorption is confirmed by the FT-IR/ATR adsorption spectra as illustrated in Figure 6. Compared are the spectra corresponding to the C_{12}TAB adsorption at silica−liquid interface for pH 5.6 and pH 10.5 at 0.1 and 0.2 M $CaCl_2$. The spectra indicate the presence of the C_{12}TAB species at silica surface at all solution conditions considered and the decrease in adsorption density at pH 10.5 and high $CaCl_2$ concentrations. From the FT-IR/ATR spectra measurements, it is also possible to determine the morphology of the surface aggregates structures by calculating the order parameter of the adsorbed surfactant film. The detailed procedure of the spectra interpretation and order parameter calculation can be found in Singh et al. (6). According to previous investigation, it is anticipated that the adsorbed surfactant moieties formed by C_{12}TAB on silica surface at concentrations above CMC will be spherical micellar aggregates (4−6, 39, 40). Indeed, the order parameter for adsorbed surfactant structures determined from s- and p-polarized FT-IR/ATR adsorption spectra at pH 5.6 and pH 10.5 with 0.1 and 0.2 M $CaCl_2$

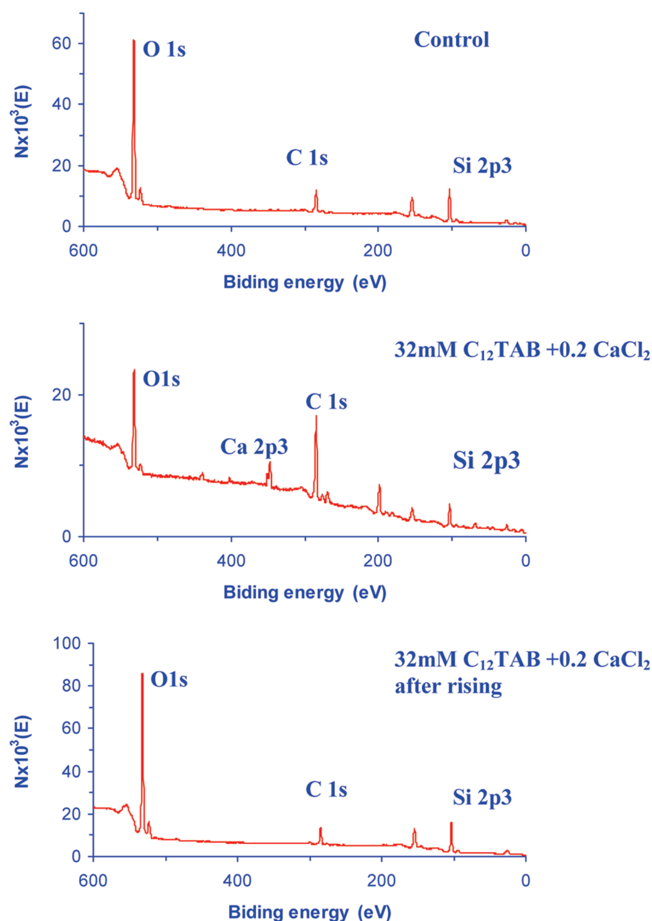

FIGURE 7. XPS spectra for (a) silica wafer before interaction with solution, (b) silica wafer that has been in contact with 32 mM $C_{12}TAB$ and 0.2 M $CaCl_2$ solution, (c) the same wafer after rinsing. Oxygen (O1s), calcium (Ca 2p3), carbon (C 1s), and silicon (Si 2p3) picks are marked in each spectrum.

were all found to be near zero. The zero-order parameter confirms the presence of random or nondirectionally oriented structures on the silica surface under the conditions investigated, consistent with spherical micellar aggregates (6).

Reversibility of Ca^{2+} Cation Adsorption. When investigating the mechanism of $CaCl_2/C_{12}TAB$ enhanced polishing rates, we considered the possibility of Ca^{2+} chemisorption to the silica surface. It has been suggested that the Ca^{2+} chemisorption is possible through a dehydration reaction between surface silanols and $CaOH^+$ ions forming a stable calcium silicate (41). To determine whether the chemisorption reaction takes place under the present conditions, we investigated the reversibility of Ca^{2+} adsorption via XPS and lateral force microscopy (LFM) measurement. In contrast to physisorbed Ca^{2+} cations that can be rinsed from the silica surface with deionized water, calcium silicate surface deposits should not readily dislodge or dissolve with water rinsing. Figure 7a presents the XPS spectra data from the surface composition of a clean silica wafer before immersion in solution (control), Figure 7b is the wafer spectra after a prolonged immersion in 32 mM $C_{12}TAB$ with 0.2 M $CaCl_2$ followed only by nitrogen gas blow drying. Figure 7c is the spectra for the same sample after careful

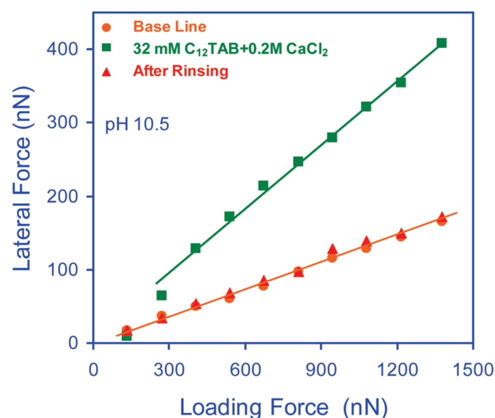

FIGURE 8. Lateral force as a function of the applied load for a 7.5 μm silica sphere interacting with a smooth silica surface in pH 10.5 aqueous solution (baseline), after solution exchange with pH 10.5 aqueous solution of 32 mM $C_{12}TAB$ and 0.2 M $CaCl_2$, and finally after ample rinsing with the baseline solution.

rinsing with pure water and drying. The Ca 2p3 peak, which can be observed on the sample after the immersion in solution, disappears after rinsing with water, indicating that the adsorption process is reversible.

The reversibility of Ca^{2+} was as well implied by some of the LFM measurements that we detail in the following section but here we would like to comment only on the adsorption reversibility control measurement set which are shown in Figure 8. Briefly, initial lateral force vs loading force measurements were conducted between a 7.5 μm silica sphere and silica wafer in pH 10.5 deionized water (baseline), identical measurements were taken after the solution exchange with pH 10.5 of 32 mM $C_{12}TAB$ with 0.2 M $CaCl_2$ and again after ample rinsing with pH 10.5 deionized water. The measurements after rinsing were essentially identical to the original baseline measurement (Figure 8). Hence, we conclude that competitive physisorption is the dominant mechanism modulating surfactant adsorption in the current research.

Lateral Interactions. Prior extensive colloidal probe LFM investigation of silica nanotribolgy in aqueous electrolyte solutions and in the presence of surfactant additives were conducted by our group (11−13) and by the group of Higashitani (36, 42−47). These works established colloidal probe LFM as a powerful and sensitive tool in investigating the molecular mechanisms during tribological engagement in complex aqueous environments. In particular, this prior research has indicated that LFM could be used to predict CMP slurries performance (11). The large range of polishing rates achievable without compromising the polishing quality in the present $C_{12}TAB/CaCl_2$ system with the change of only one principal parameter ($CaCl_2$ concentration) make it an excellent model system for demonstrating the utility of LFM in the design and analysis of CMP slurries for optimum performance.

The results of the LFM experiments are presented in Figure 9. The impact of $CaCl_2$ on the friction encountered during particle-wafer contact was investigated by measuring the lateral force between a silica sphere and the wafer surface over a range of loading forces and solution condi-

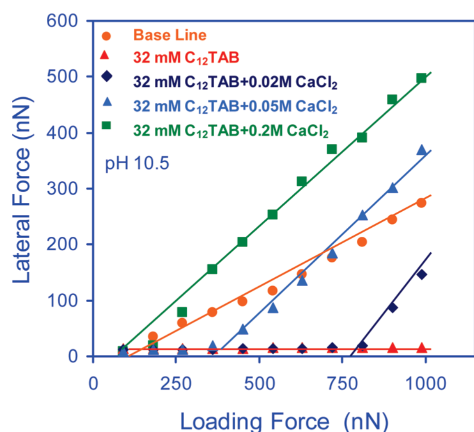

FIGURE 9. Lateral force as a function of the applied load for a 7.5 μm silica sphere interacting with a smooth silica surface in pH 10.5 pure aqueous solution (baseline), and in pH 10.5 aqueous solutions of 32 mM $C_{12}TAB$ without or with the addition of 0.02, 0.05, and 0.2 M $CaCl_2$. The slopes of the strait solid lines drawn to guide the eye are proportional to the friction coefficients values in each range.

tions relevant to CMP processes and in particular to the applied pressures used in the polishing test as well as the normal force measurement detailed in the previous sections. Initial reference measurement were taken in the baseline solution of pH 10.5 pure water and presents a characteristic linear increase of the friction force with the applied load for the investigated loading force range. The introduction of 32 mM $C_{12}TAB$ solution significantly reduces the load dependent lateral force response due to surfactant mediated boundary lubrication as demonstated previously and in accordance with the negligible removal rates observed in the polishing test. Note that the load range applied in these measurements far exceeds the critical loads necessary to break the surface aggregates so the surfactant mediated boundary lubrication is provided by the residual surfactant layer trapped between the particle and the surface after the destruction of micellar aggregates. For the case of $C_{12}TAB$ solutions without Ca^{2+} cations, the friction coefficient (or the slope of the lateral force vs load dependence plotted in Figures 8 and 9) remains very low for the entire range of applied loads. A different dependence is observed for the case of $C_{12}TAB$ in the presence of $CaCl_2$, in which case the measurements indicate the presence of a critical loading force above which the friction coefficient abruptly changes. This abrupt change is believed to signify sudden boundary layer lubricant breakdown resulting in a transition between surfactant-mediated lubrication to bare surface engagement in the presence of Ca^{2+} cations. It is important to note that the critical loading force for boundary lubrication breakdown is systematically modified by the addition of increasing concentrations of $CaCl_2$. Hence, by the addition of $CaCl_2$ to a $C_{12}TAB$ lubricated silica system, it is possible to precisely engineer the applied load at which enhance frictional engagement commences.

The increase in the friction force in the presence of $CaCl_2$ is in general agreement with prior measurement of the friction between silica surfaces in pure electrolyte solutions. Monovalent cations (Li^+, Na^+, Cs^+) act as boundary lubricants (32), but bivalent cations exhibit a more complex behavior with some of them (Ba^{2+}, Sr^{2+}) acting as good lubricants and others (Mg^{2+}) as friction enhancers for silica−silica interactions (44). The type of the anion is also important in the case of bivalent cationic salts. In particular at normal pH $Ca(NO_3)_2$ is a good lubricant, whereas $CaCl_2$ increases friction with increasing electrolyte concentration and this effect is further enhanced at higher pH (45−47).

The present results suggest that the regulation of $C_{12}TAB$/$CaCl_2$ mediated silica CMP removal rate is accomplished through the completive adsorption of the lubricating $C_{12}TAB$ aggregates and the friction enhancing Ca^{2+} cations. It should be noted that subsequent to boundary layer lubrication breakdown, the friction coefficients in the presence of Ca^{2+} in the surfactant systems is greater than in the case of bare silica interactions across pH 10.5 DI water. The results from the previous section support that this phenomena is most probably not related to chemical complexation of Ca^{2+} at the silica surface. However, the presence of Ca^{2+} ion could weaken Si−O−Si bonds and hence are thought to promote the chemo-mechanical wear mechanism in silica CMP (17, 18). The exact physical mechanism by which the Ca^{2+} cations enhance the friction between silica surfaces and the respective material removal rates is out of the scope of the present paper and will be addressed in future publications. In the context of the present investigation, an important outcome is that the enhanced lateral force response observed in the presence of calcium correlates well with the enhanced polishing removal rate as indicated by comparing the data in Table 1 and Figure 9.

CONCLUSIONS

The influence of Ca^{2+} cation addition on dodecyl trimethylammonium bromide ($C_{12}TAB$) mediated lubrication of silica surfaces has been examined via atomic force microscopy, lateral force microscopy, benchtop polishing experiments, and surfactant adsorption studies. It is demonstrated that the introduction of ions into solution that modulate the surfactant headgroup-surface electrostatic affinity can be used to tune friction and wear without compromising dispersion. Colloidal probe AFM interaction force measurements in conjunction with LFM and surfactant adsorption studies demonstrated that Ca^{2+} cations physically compete with $C_{12}TAB$ surfactant for electrostatic binding sites at the silica surface. This competition is believed to result in a weakened affinity of adsorbed surfactant structures to the silica, enabling pressure sensitive boundary layer breakdown. The critical pressure for lubrication breakdown was demonstrated to be reversible and tunable with Ca^{2+} cation concentration.

To the best of our knowledge, the present research represents the first example of a self-healing, reversible, and pressure tunable tribological system for use in an aqueous environment. The general principles developed here for the case of CMP slurries optimization are anticipated to lead to smart lubrication schemes for an enhanced performance in a wide variety of processes. The ability to control the extent of lubrication mediated by surfactant structures, in particle technologies alone, has the potential of enhancing the

performance of numerous unit operations including traditional processes such as communition, dewatering and filtration, high speed coatings, and the pumping and transport of concentrated slurries. Such lubrication schemes will also prove advantageous for MEMS and NEMS systems where selective lubrication could result in enhance device lifetime and improved performance.

Acknowledgment. The authors acknowledge the financial support of the Particle Engineering Research Center (PERC) and Center for Particulate and Surfactant Systems (CPASS) at the University of Florida, The National Science Foundation (NSF) (Grant EEC-94-02989; IIP-0749481), and the Industrial Partners of PERC for support of this research. Any opinions, findings and conclusions or recommendations expressed in this material are those of the author(s) and do not necessarily reflect those of the National Science Foundation.

REFERENCES AND NOTES

(1) Russel, W. B.; Saville, D. A.; Schowalter, W. R. *Colloidal Dispersions*; Cambridge University Press: New York, 1989.
(2) Rosen, M. J. *Surfactants and Interfacial Phenomena*, 2nd ed.; Wiley: New York, 1989.
(3) *Surfactants in Personal Care Products and Decorative Cosmetics*, 3rd ed.; Rhein, L. D., O'Lenick, A., Schlossman, M., Somasundaran, P., Eds.; Taylor & Francis Group: Abingdon, U.K., 2006.
(4) Adler, J. J.; Singh, P. K.; Patist, A.; Rabinovich, Y. I.; Shah, D. O.; Moudgil, B. M. *Langmuir* **2000**, *16*, 7255.
(5) Subramaniam, V.; Ducker, W. A. *Langmuir* **2000**, *16*, 4447.
(6) Singh, P. K.; Adler, J. J.; Rabinovich, Y. I.; Moudgil, B. M. *Langmuir* **2001**, *17*, 468.
(7) Vakarelski, I. U.; Toritani, A.; Nakayama, M.; Higashitani, K. *Langmuir* **2003**, *19*, 110.
(8) Atkin, R.; Craig, V. S. J.; Wanless, E. J.; Biggs, S. *Adv. Colloid Interf. Sci.* **2003**, *103*, 219.
(9) Rabinovich, Y. I.; Vakarelski, I. U.; Brown, S. C.; Singh, P. K.; Moudgil, B. M. *J. Colloid Interface Sci.* **2004**, *270*, 29.
(10) Schniepp, H. C.; Saville, D. A.; Aksay, I. A. *J. Am. Chem. Soc.* **2006**, *128*, 12378.
(11) Basim, G. B.; Vakarelski, I. U.; Moudgil, B. M. *J. Colloid Interface Sci.* **2003**, *263*, 506.
(12) Basim, G. B.; Brown, S. C.; Vakarelski, I. U.; Moudgil, B. M. *J. Dispersion Sci. Technology* **2003**, *24*, 499.
(13) Vakarelski, I. U.; Brown, S. C.; Rabinovich, Y. I.; Moudgil, B. *Langmuir* **2004**, *20*, 1724.
(14) Briscoe, W. H.; Titmuss, S.; Tiberg, F.; Thomas, R. K.; McGillivray, D. J.; Klein, J. *Nature* **2006**, *444*, 191.
(15) Drummond, C.; Marinov, G.; Richetti, P. *Langmuir* **2008**, *24*, 1560.
(16) Beauvais, M.; Serreau, L.; Heitz, C.; Barthel, E. *J. Colloid Interface Sci.* **2009**, *331*, 178.
(17) Cook, L. M. *J. Non-Cryst. Solids* **1990**, *120*, 152.
(18) Singh, R. K.; Lee, S. M.; Choi, K. S.; Basim, G. B.; Choi, W. S.; Chen, Z.; Moudgil, B. M. *MRS Bull.* **2002**, *27*, 752.
(19) Maw, W.; Stevens, F.; Langford, S. C.; Dickinsona, J. T. *J. Appl. Phys.* **2002**, *92*, 5103.
(20) Liang, H.; Craven, D. *Tribology in Chemical Mechanical Planarization*; CRC Press: Boca Raton, FL, 2005.
(21) *Microelectronic Applications of Chemical Mechanical Planarization*; Li, Y., Ed; Wiley-Interscience: Hoboken, NJ, 2008.
(22) Raghavan, S.; Keswani, M.; Jia, R. *KONA Powder Part.* **2008**, *26*, 94.
(23) Krishnan, M.; Nalaskowski, J. W.; Cook, L. M. *Chem. Rev.* **2010**, *110*, 178.
(24) Shah, K.; Chiu, P.; Jain, M.; Fortes, J.; Moudgil, B. M.; Sinnott, S. *Langmuir* **2005**, *21*, 5337.
(25) Shah, K.; Chiu, P.; Sinnott, S. B. *J. Colloid Interface Sci.* **2006**, *296*, 342.
(26) Cleveland, J. P.; Manne, S.; Bocker, D.; Hansma, P. K. *Rev. Sci. Instrum.* **1993**, *64*, 1.
(27) Butt, H.-J.; Cappella, B.; Kappl, M. *Surf. Sci. Rep.* **2005**, *59*, 1.
(28) Bhushan, B. *Handbook of Micro/Nanotribology*, 2nd ed.; CRC Press: Boca Raton, FL, 1995.
(29) Carpick, R. W.; Salmeron, M. *Chem. Rev.* **1997**, *97*, 1163.
(30) Bogdanovic, G.; Meurk, A.; Rutland, M. W. *Colloids Surf., B* **2000**, *19*, 397.
(31) Franks, G. V.; Colic, M.; Fisher, M. L.; Lange, F. *J. Colloid Interface Sci.* **1997**, *193*, 96.
(32) Colic, M.; Fisher, M. L.; Franks, G. V. *Langmuir* **1998**, *14*, 2207.
(33) Franks, G. V.; Johnson, S. B.; Scales, P. J.; Boger, D. V.; Healy, T. W. *Langmuir* **1999**, *15*, 4411.
(34) Vakarelski, I. U.; Ishimura, K.; Higashitani, K. *J. Colloid Interface Sci.* **2000**, *227*, 111.
(35) Vakarelski, I. U.; Higashitani, K. *J. Colloid Interface Sci.* **2001**, *242*, 110.
(36) Donose, B. C.; Vakarelski, I. U.; Higashitani, K. *Langmuir* **2005**, *21*, 1834.
(37) Tadros, Th. F.; Lyklema, J. *J. Electroanal. Chem.* **1969**, *22*, 1.
(38) James, R. O.; Healy, T. W. *J. Colloid Interface Sci.* **1972**, *40*, 45.
(39) Manne, S.; Gaub, H. E. *Science* **1995**, *270*, 1480.
(40) Liu, J.-F.; Ducker, W. A. *J. Phys. Chem. B* **1999**, *103*, 8558.
(41) Greenberg, S. A. *J. Phys. Chem.* **1956**, *60*, 325.
(42) Taran, E.; Donose, B. C.; Vakarelski, I. U.; Higashitani, K. *J. Colloid Interface Sci.* **2006**, *297*, 199.
(43) Donose, B. C.; Taran, E.; Vakarelski, I. U.; Shinto, H.; Higashitani, K. *J. Colloid Interface Sci.* **2006**, *299*, 233.
(44) Donose, B. C.; Vakarelski, I. U.; Taran, E.; Shinto, H.; Higashitani, K. *Ind. Eng. Chem. Res.* **2006**, *45*, 7035.
(45) Taran, E.; Kanda, Y.; Vakarelski, I. U.; Higashitani, K. *J. Colloid Interface Sci.* **2007**, *307*, 425.
(46) Donose, B. C. PhD Thesis. Kyoto University, Kyoto, Japan, 2005.
(47) Taran, E. PhD Thesis. Kyoto University, Kyoto, Japan, 2006.

AM100070E